Magnetic resonance functional neuroimaging: New insights into the human brain

Jens Frahm*

Biomedizinische NMR Forschungs GmbH am Max-Planck-Institut für biophysikalische Chemie, D-37070 Göttingen, Germany

Magnetic resonance (MR) functional neuroimaging emerges as a new tool for mapping human brain functions at unsurpassed spatial resolution. The technique is noninvasive, widely available, and applicable to single subjects. Despite its tremendeous potential in cognitive neuroscience, ongoing methodologic developments pose significant challenges. They are mostly caused by the fact that MR detection of a focal change of brain activity is indirect and therefore relies on an unaffected neurovascular and/or neurometabolic coupling. This article describes some of the crucial elements necessary to transform a paradigm-related change in brain activity into a corresponding MR activation map. Pertinent examples range from data acquisition and signal processing to the underlying physiological mechanisms and details of the paradigm design.

OVER the past 15 years, the evolution of magnetic resonance imaging (MRI) has witnessed tremendous progress. Scientific and clinical investigations aiming at new insights into the intact human body have made MRI the premier modality for a delineation of structural anatomy at high spatial resolution and with exquisite soft tissue contrast[1]. Beyond mere morphologic studies, more recent advances extend the arsenal of evaluations to cellular metabolism by localized magnetic resonance spectroscopy (MRS) and thus add a biochemical dimension to diagnostic imaging[2]. Even functional characteristics became available such as magnetic resonance angiography, tissue perfusion, diffusion contrast, and magnetization transfer techniques. However, the most fascinating development is the discovery that suitable MRI techniques will allow us to map human brain functions, i.e. to visualize the actual process of thinking.

Experimental work in animals first demonstrated that the level of cerebral blood oxygenation (CBO) influences the signal intensity of T_2*-weighted gradient-echo MR images[3,4]. Whereas oxyhemoglobin is diamagnetic, deoxygenated hemoglobin may serve as an endogeneous paramagnetic contrast agent that causes dephasing of water proton spins in its direct vicinity. The physical effect is a signal loss when MRI detection integrates pertinent magnetizations over an image pixel. The degree of signal loss depends on the absolute concentration of deoxyhemoglobin per voxel and scales with voxel size and gradient-echo time, i.e. the differential precession of spin moments between excitation and detection. For example, if an increase in cerebral blood flow and oxygenation decreases the deoxyhemoglobin concentration, then both the effective spin–spin relaxation time T_2* and the corresponding signal intensity of a gradient-echo image show a concomitant increase. This CBO or blood oxygenation level dependent (BOLD) contrast may be enhanced by acquiring the images at prolonged echo times of, for example, 30 to 50 ms.

The demonstration of oxygenation sensitivity in animal imaging was rapidly followed by the observation that BOLD contrast may be exploited for functional mapping of the human brain[5–9]. The underlying mechanism is due to the fact that a change in neuronal activity – often termed activation – is accompanied by a rise in cerebral blood flow that at least transiently 'uncouples' from oxygen consumption[10,11] and therefore results in a venous hyperoxygenation, i.e. decreased deoxyhemoglobin. Although the full details of the hemodynamic and metabolic correlates associated with brain activation are not yet fully understood, the initial signal intensity rise after stimulus onset is easily observable and well documented for visual, auditory, and sensorimotor cortical processing.

The use of MR functional neuroimaging is attractive because of several reasons: it is noninvasive and offers repeated studies of individual subjects at unsurpassed spatiotemporal resolution and with a high degree of flexibility in the design of cognitive paradigms. Moreover, high-field MRI is widely distributed and less costly than positron emission tomography systems. On the other hand, and similar to other functional neuroimaging modalities, MRI studies of brain function rely on 'secondary signals' that link changes in neuronal activity to correlated alterations of metabolism (e.g. glucose and oxygen consumption), perfusion (blood flow and blood volume), and blood oxygenation. In fact, the techniques mainly focus on perfusion-related changes of the intravascular concentration of deoxygenated and therefore paramagnetic hemoglobin. Figure 1 schematically sketches the path from a change in focal neuronal

*For correspondence. (e-mail: jfrahm@gwdg.de)

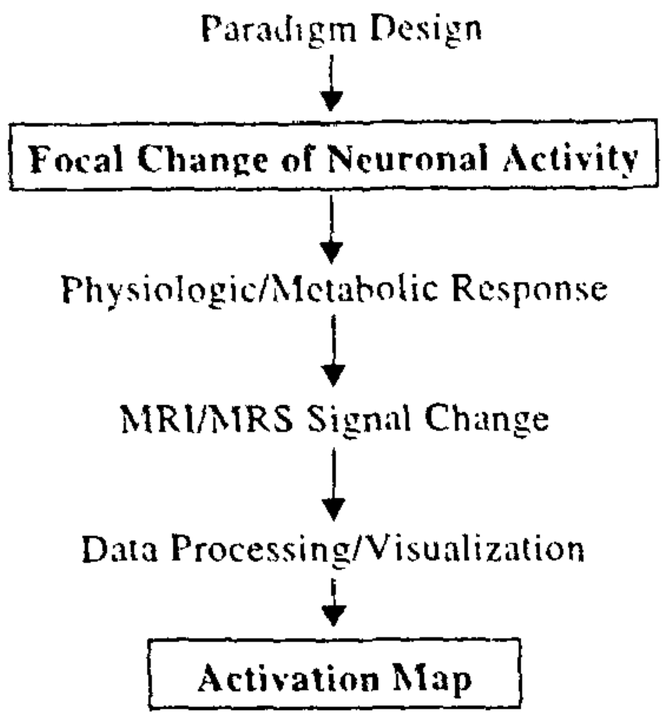

Figure 1. Schematic diagram demonstrating the transformation of a focal change of neuronal activity into an activation map. MRI responses to brain activation (i) reflect differences in the experimental paradigm and its particular design, (ii) are sensitive to modulations of the neruovascular and/or neurometabolic coupling, and (iii) may be influenced by technical aspects of data acquisition and data processing including visualization and statistical treatment.

activity to an MRI-derived activation map and clearly indicates putative interferences at several levels ranging from data acquisition and signal processing to physiologic mechanisms and details of the paradigm design.

Thus, a key to understanding MR functional neuroimaging is the fact that it does not measure neuronal activity directly. The crucial question therefore is: how can we reliably detect a change in neuronal activity at the physiologic level? To answer this question we need to examine the neurovascular and neurometabolic coupling under various experimental and clinical conditions, e.g. with respect to confounding modulations caused by medication, brain disease, or even paradigm timings, and to carefully optimize the MRI strategies. Following the concept outlined in Figure 1, the purpose of this article is to briefly cover some of the crucial aspects involved in successfully mapping brain activation by MRI.

Technical aspects

Basic MRI sequences and functional contrast

Depending on the desired spatial or temporal resolution we employ FLASH or single-shot EPI sequences with prolonged echo times, respectively. Basic radiofrequency and gradient sequences are shown in Figure 2. Typically, EPI sequences acquire all differently phase-encoded gradient echoes required for image reconstruction after a single slice-selective RF excitation pulse. The individual echoes are generated by multiple sinusoidal or trapezoidal reversal of the read or frequency-encoding gradient. Phase encoding is most conveniently accomplished by a 'blipped' gradient, whereas the

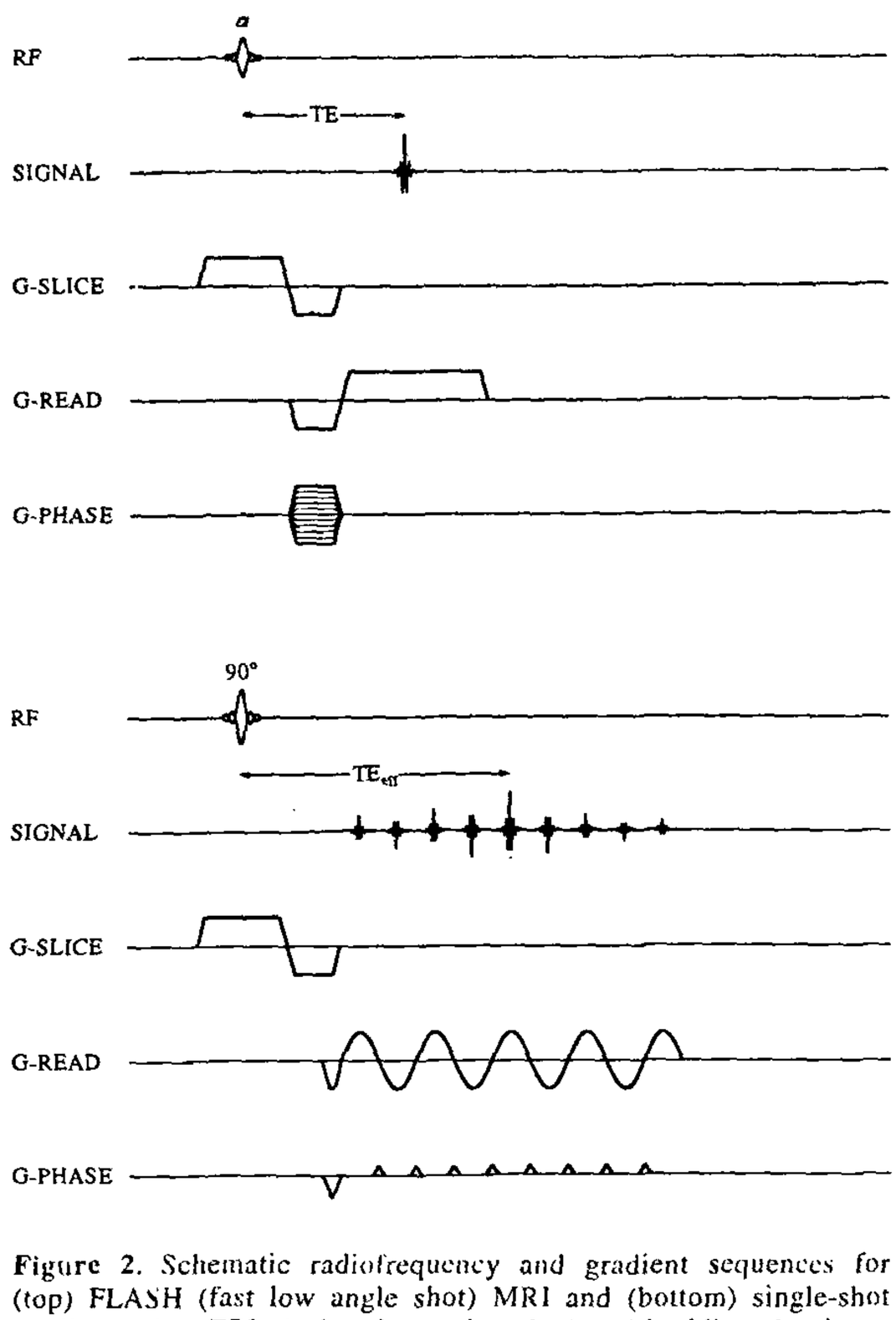

Figure 2. *Schematic radiofrequency and gradient sequences for* (top) FLASH (*fast low angle shot*) MRI and (bottom) single-shot gradient-echo EPI (echo-planar imaging) with blipped phase-encoding and symmetric coverage of *k* space. EPI sequences acquire all differently phase-encoded (G-PHASE) gradient echoes (SIGNAL) after a single RF excitation pulse (RF) in conjunction with a slice select gradient (G-SLICE), whereas FLASH sequences employ multiple RF pulses with low flip angles $\alpha < 90°$ and generate only a single gradient echo per repetition interval by inversion of the frequency-encoding read gradient (G-READ).

original EPI technique used a weak constant gradient. Because the echoes cover a large range of different echo times, the effective TE value is given by the Fourier line representing the lowest spatial frequency, i.e. for zero phase encoding, as it dominates image contrast. EPI emphasis is on high speed yielding imaging times of the order of 100 ms and excellent volume coverage by multi-slice imaging at the expense of limited in-plane resolution.

In contrast, FLASH sequences require multiple RF excitations with low flip angles $\alpha < 90°$ and normally generate only a single gradient echo per repetition interval. As large TE values also prolong the repetition time, typical imaging times are in the range of several seconds. The ability to select an arbitrary compromise between temporal and spatial resolution is best exploited for gaining access to high-resolution maps at the expense of volume coverage. Pertinent applications there-

fore provide a complementary strategy to EPI. As demonstrated below, the images suffer also less artifacts than EPI because of their conventional way of covering the *k* space and their use of a fixed time for all gradient echoes.

Motion and susceptibility artifacts

Functional information about the human brain is extracted from serial MR images acquired over a period of several minutes and during a paradigm that compares at least two different conditions. Simple examples are visual stimulations, finger motor tasks, or silent word generations. As a consequence, mathematical methods that compare signal intensity time courses on a pixel-by-pixel basis to identify task-related changes strongly depend on the assumption that no other changes have occurred. In particular, this refers to signal fluctuations induced by vascular flow and even slow involuntary subject movements. For both FLASH and EPI, it is therefore recommended to adjust flip angles and repetition times such as to avoid T_1-weighting and thereby minimize the sensitivity to amplitude fluctations[12]. Although these precautions together with an optimized gradient waveform design and/or the use of navigator echoes help to control flow effects from large vessels and intrascan motions, a residual problem may result from stimulus-correlated movements that are often due to a slight nodding of the subject's head or represent a continuous drift during the experimental time. Whereas the latter may be corrected retrospectively, the former influence may even be difficult to detect unless major motions lead to a spatially unspecific emphasis of all contrast borders in the resulting activation map. In any case, it may be advisable to control the raw image series by a rapid cine display.

Figure 3 shows spin–density weighted EPI and FLASH images with T_2* sensitivity that are used in our laboratory for functional mapping. For a fixed field-of-view of 200 mm the images illustrate the achievable image quality and contrast for pixel matrices of 64 × 64, 128 × 128, and 256 × 256 (FLASH only) in comparison to a flow-sensitized anatomic FLASH image of the same section. Even in this 'good' transverse section with few macroscopic magnetic field inhomogeneities high up in the head, the presence of small susceptibility differences, e.g. at the borderline of the frontal brain, causes

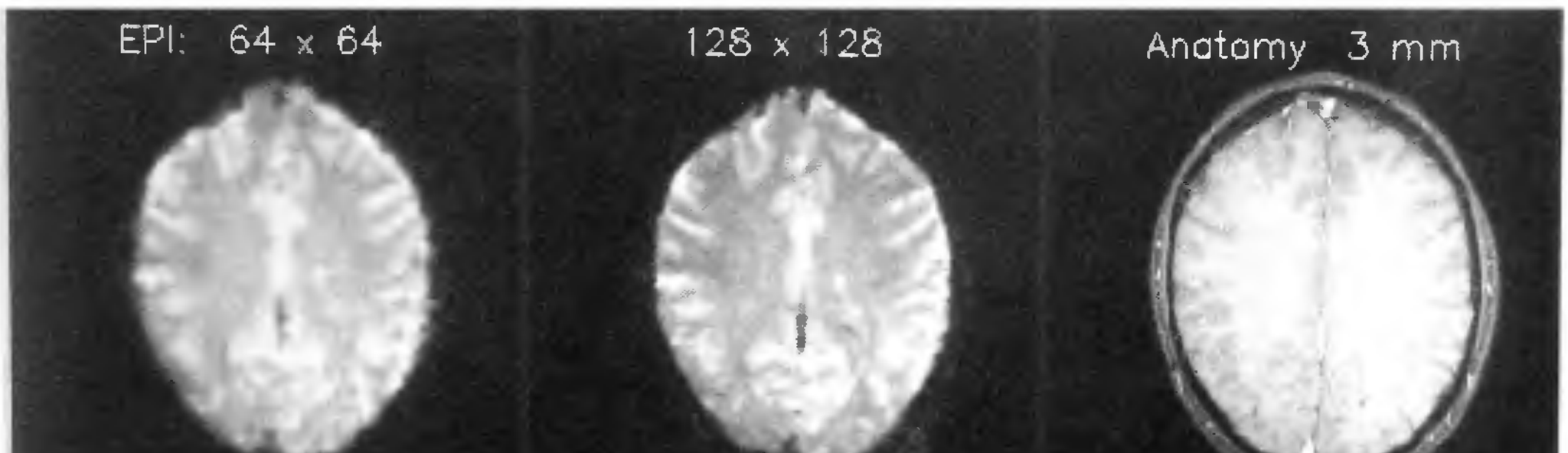

Figure 3. Basic contrast and spatial resolution of (top) EPI and (bottom) FLASH images commonly employed for functional neuroimaging at 2.0 Tesla (Siemens Vision) in comparison to a flow-sensitized anatomic FLASH image of the same section (top right). Imaging parameters were adjusted to avoid T_1 weighting and to ensure spin–density contrast, i.e. TR = 6000 ms and flip angle 90° for EPI and TR = 62.5 ms and flip angle 10° for FLASH, in combination with T_2* sensitivity, i.e. an effective TE = 54 ms for EPI and TE = 30 ms for FLASH.

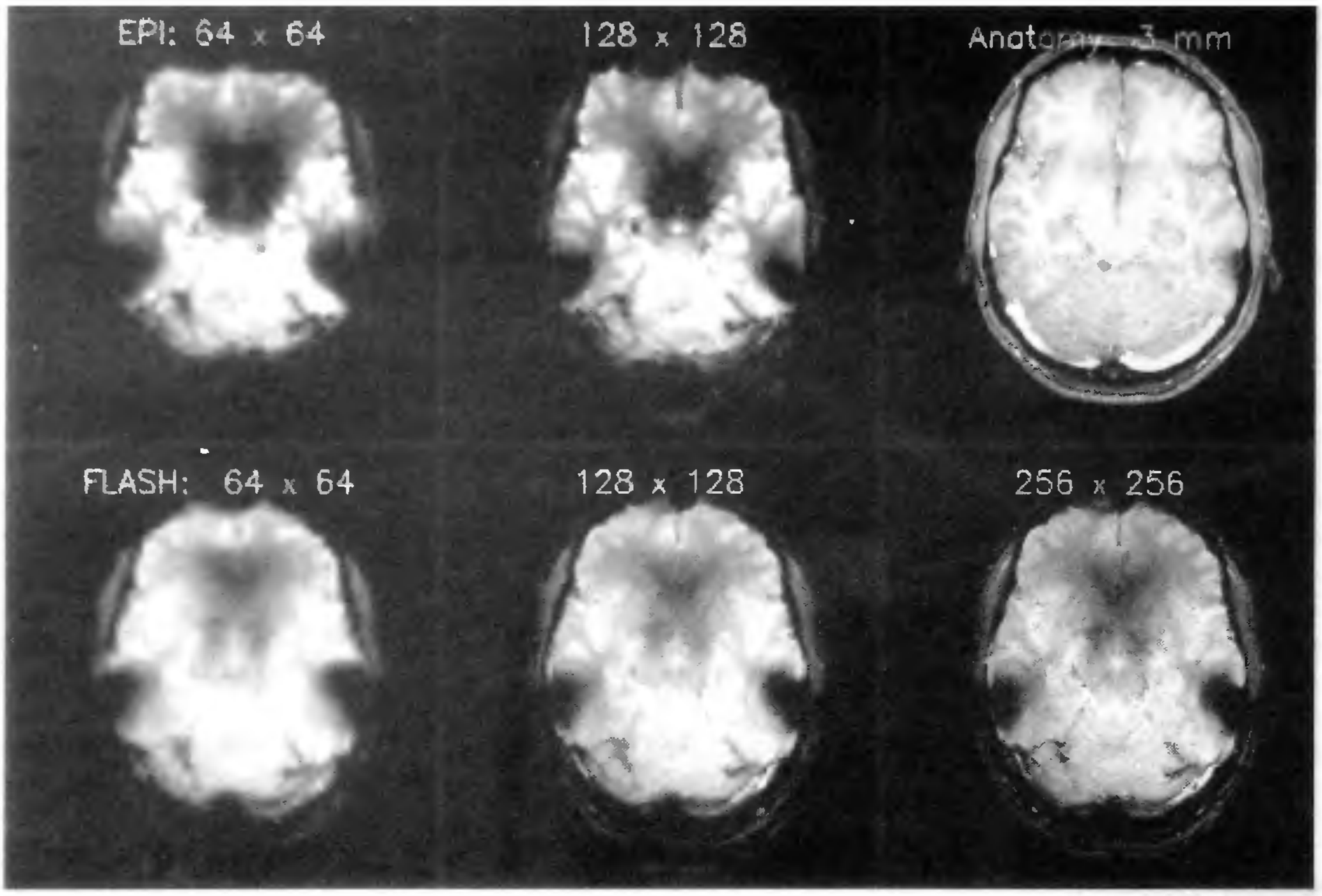

Figure 4. Macroscopic susceptibility effects caused by air–tissue interfaces in (top) EPI and (bottom) FLASH images commonly employed for functional neuroimaging at 2.0 Tesla (Siemens Vision) in comparison to a flow-sensitized anatomic FLASH image of the same section (top right). The data originate from the same subject as in Figure 3 using identical imaging parameters except for choosing a section through the lower part of the brain. The artifacts represent signal losses (EPI, FLASH) and geometric distortions (EPI) that increase with pixel size, i.e. reduced spatial resolution.

partial signal loss and geometric distortions in the low-resolution 64 × 64 EPI but not FLASH image.

Inhomogeneity problems become dramatic while moving to a 'bad' section through the lower part of the brain which is characterized by the presence of strong magnetic susceptibility differences due to air–tissue interfaces, e.g. near the ear canals and nasal cavities. Figure 4 clearly demonstrates that the sensitivity to unwanted structural inhomogeneities will remain a key problem for MR functional neuroimaging unless effective compensation strategies can be developed that overcome the dominating influence of the miscalibrated slice selection gradient[13]. The image artifacts are only partially compensated for by the use of very small voxel sizes, i.e. very high spatial resolution and thin sections, which reduce the extent of signal dephasing within an image voxel but retain the wanted sensitivity to deoxyhemoglobin-induced susceptibility differences[14]. In fact, in contrast to the macroscopic nature of most structural susceptibility differences, the magnetic field variations around the microvasculature are microscopic in nature, (e.g. less than 50 μm) and well below the size of a typical image voxel (e.g. 1 mm).

Data evaluation and visualization

Figure 5 summarizes some of the elements of a simple visual mapping experiment using FLASH MRI at 2.0 tesla (Siemens Vision). Definition of section orientation, anatomy, and vasculature (top panels) is followed by dynamic acquisitions of spin–density weighted images with T_2* sensitivity of 6 s temporal resolution and $0.78 \times 0.78\ mm^2$ spatial resolution (middle panels). Relative to darkness, raw images during flickerlight stimulation reveal a focal increase in MRI signal intensity, i.e. a decrease in deoxyhemoglobin, in selected areas of visual cortex.

In principle, there are many ways of extracting functional information from dynamic image series and to identify activated pixels in corresponding maps. Apart from the use of various forms of temporal or spatial filters (not applied here) and post-acquisition motion or 'baseline' correction schemes (also not applied here), the possibilities include the analysis of signal differences, variances, statistical parameters, temporal correlations or frequencies, principal components, clusters, phase information, and noise characteristics: neither is

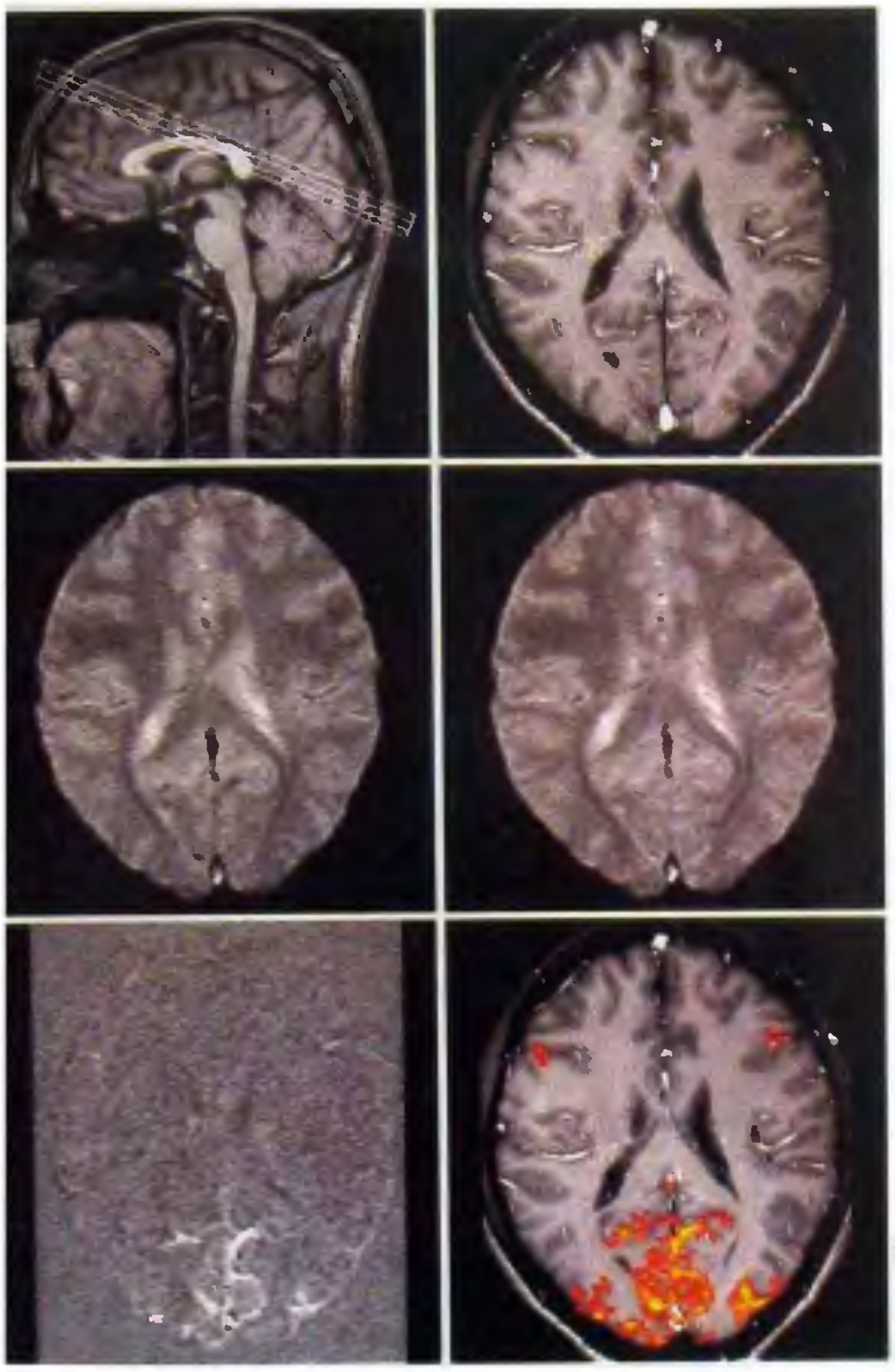

Figure 5. Functional mapping of visual stimulation. (Top left) Definition of section orientation (2.0 T, Siemens Vision, 3D FLASH, TR/TE = 15/6 ms, flip angle 20°) and (top right) section anatomy and vasculature (FLASH, TR/TE = 70/6 ms, flip angle 50°) in a normal volunteer. In going from darkness (middle left) to flickerlight stimulation (middle right), dynamic acquisitions of spin–density weighted FLASH images with T_2* sensitivity (FLASH, 96 × 256 matrix, rectangular FOV 150 × 200 mm^2, slice thickness 4 mm, TR/TE = 62.5/30 ms, flip angle 10°, measuring time 6 s) reveal a focal increase in MRI signal intensity, i.e. a decrease in deoxyhemoglobin, in visual cortex. (Bottom left) Difference map and (bottom right) colour-coded activation map calculated by a pixel-by-pixel cross-correlation of signal intensity time courses with a reference vector that represents the stimulus protocol, compare Figure 6. (Modified from Kleinschmidt, A. *et al.*, *Int. J. Imag. Syst. Technol.*, 1995, **6**, 238–244).

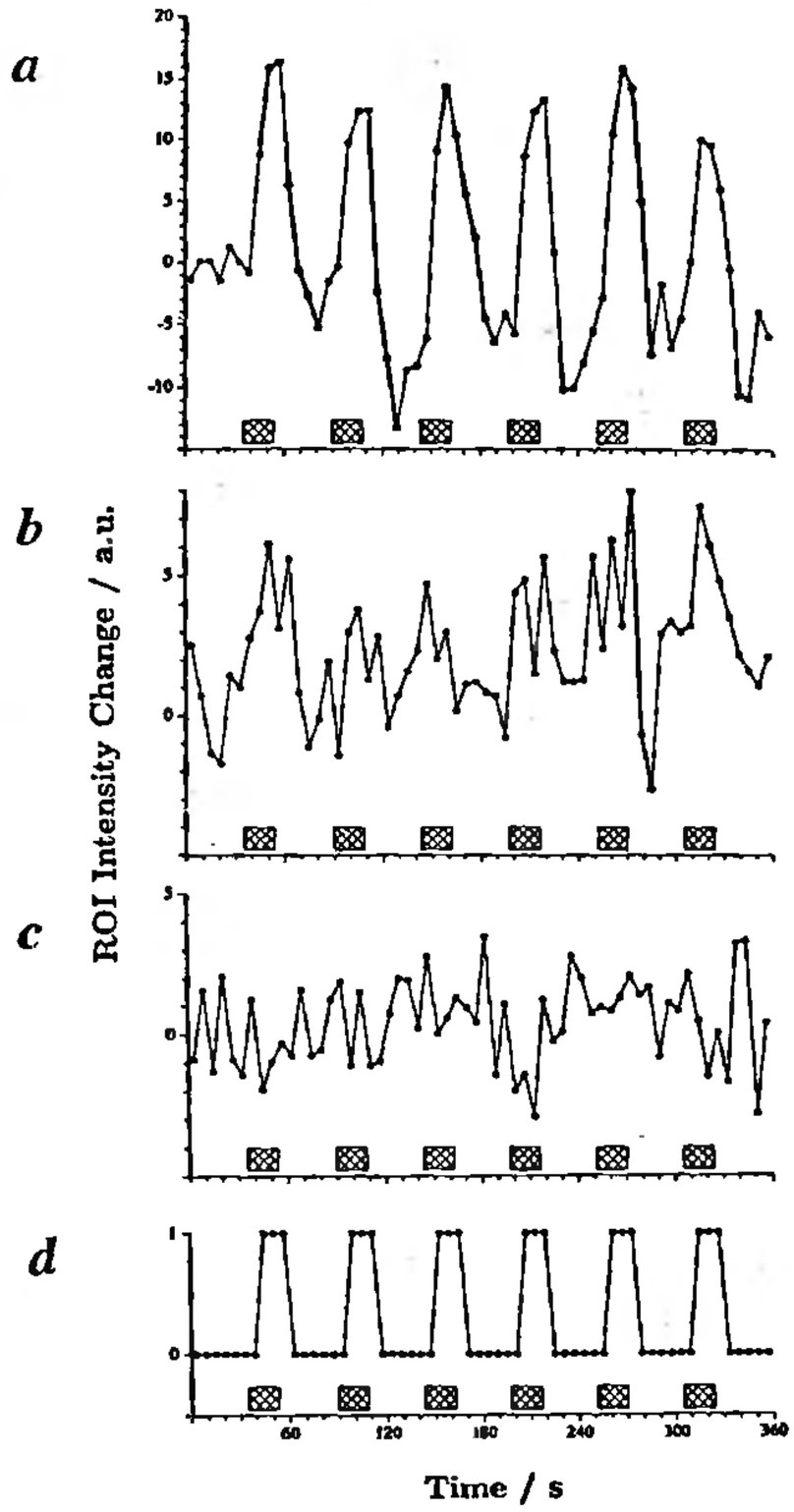

Figure 6 *a–d*. Normalized time courses of oxygenation-sensitive MRI signal intensities (2.0 T, FLASH, TR/TE = 62.5/30 ms, flip angle 10°, temporal resolution 6 s) from regions-of-interest in *a*, primary visual cortex; *b*, frontal eye field; and *c*, nonactivated frontal gray matter (control) of a single subject in response to visual activation (18 s of flickerlight vs 36 s of darkness). *d*, Reference function that mimics the temporal structure of the stimulation protocol shifted by one image (6 s) to account for hemodynamic latencies. This boxcar function was employed to calculate the threshold map of cross-correlation coefficients shown in Figure 5. (Modified from Kleinschmidt, A. *et al.*, *Der Radiologe*, 1995, **35**, 242–251).

this list complete nor is a comprehensive description within the scope of this article. As shown in the bottom left part of Figure 5, the most simple approach is time-locked averaging of images and subsequent subtraction across functional states, i.e. summation of images that are acquired during one condition, (e.g. lights off) and subtraction of the result from that obtained for a different condition (e.g. lights on). The resulting difference map will show cortical areas that are involved in processing flickerlight relative to darkness. Whether the CBO responses reflect the enhanced firing or synchronization of neurons or – more likely – indicate the recruitment of new, though overlapping populations of specialized neurons within the visual cortex cannot be decided from the MRI experiment alone. We need to keep in mind that even high-resolution studies in general are too coarse to resolve the columnar organization of the human cortex. Moreover, quantification and calibration of MRI signals, amplitude differences, or even T_2* relaxation rates are precluded because of the influence of many experimental parameters.

A much more robust and sensitive approach than image subtraction stems from a correlation analysis that

exploits the temporal structure of the known stimulation protocol and compares it to the oxygenation-sensitive MRI signal intensity time courses on a pixel-by-pixel basis[15]. Such strategies eliminate any statistical signal fluctuations as a source of contrast and are most helpful when recording multiple stimulation cycles that alternate between conditions. Figure 6 depicts selected time courses from the primary visual cortex, frontal eye field, and non-activated frontal gray matter for the experiment shown in Figure 5. The time courses reveal stimulus-induced responses to visual activation that tightly follow the 6-fold application of a cycle comprising 18 s of flickerlight (inserted boxes) and 36 s of darkness. The bottom trace refers to a reference vector that mimics the temporal structure of the protocol shifted by one image (6 s) to account for hemodynamic latencies of the flow-induced change in CBO. This boxcar function was employed to calculate the colour-coded activation map shown in the bottom right panel of Figure 5.

The map shown represents a thresholded map of correlation coefficients that – based on the underlying noise distribution of correlation coefficients – employs a 99.99% threshold for identifying significant centers of activation and then admits directly neighbouring pixels until a lower threshold is reached for optimum area delineation[16]. In contrast to the difference map, it unambiguously highlights the activation of both frontal eye fields in this subject and section. Macroscopic veins that may blur the topographic specificity of stimulus-related activations are identified by overlay on a flow-sensitized anatomic image. However, a congruent control of the macrovasculature requires functional and morphologic maps with identical spatial resolution, a condition often not met for EPI studies.

Physiological aspects

The critical link between a focal change in neuronal activity and MRI-detectable observables is the neurovascular and/or neurometabolic coupling. Modulations of the hemodynamically driven BOLD contrast may result from intrasubject and intersubject differences in task performance, e.g. caused by arousal, attention, alertness, adaptation, sleep, or consciousness, or reflect age and gender differences. In fact, all means that affect the vascular 'responsiveness' are likely to interfere with oxygenation-sensitive mapping techniques. Obvious examples are direct pharmacologic interventions with use of psychotropic drugs such as diazepam or metamphetamine[17], or vasoactive drugs such as aminophylline or acetazolamide[18]. Anesthesia may be another complication and cerebrovascular disease has already been demonstrated to completely disrupt the expected MRI response[19]. Apart from these external interactions, there may be more subtle stimulus and brain system dependencies supported by known differences in neuroanatomy, vasculature and neurotransmitter systems. The question therefore arises whether at all or under what circumstances there is something like a characteristic oxygenation-sensitive MRI response function.

The visual response function

To answer the above question we have systematically studied the influence of protocol timings on the spatio-temporal response characteristics in the visual system. Pertinent investigations were motivated by findings for sustained visual stimulation (6 min) that reveal apparent differences between tonic and phasic MRI responses to activation[20]. This particularly applies to the identification of a slow physiologic process that complements the initial signal rise after the onset of activation. The rapid positive BOLD response is usually ascribed to a rapid increase in blood flow, i.e. oxygen delivery, not matched by a corresponding upregulation of oxidative metabolism, i.e. oxygen consumption. In contrast, the observed slow signal change refers to an attenuation of the hemodynamic response curve during the ongoing stimulation and the occurrence of a pronounced signal undershoot at the end of the stimulation. The undershoot is well below pre-stimulation baseline and requires a recovery time of almost 60 s.

Independent of the underlying mechanisms, e.g. the delayed upregulation of oxidative glucose consumption[11] or a slow modulation of the venous blood volume ('balloon' model)[21], the existence of two processes with different time constants is directly relevant for mapping studies based on much shorter protocol timings. For example, the time course data shown in Figure 6 *a* reveal a 'baseline drift' during repetitive stimulation that reaches a new steady state after about 2 min. This observation is in close agreement with the aforementioned slow physiologic process and seems to represent the consequence of accumulating undershoot contributions from preceeding stimulations[8]. Fortunately, a comparison of activation maps from sustained and repetitive protocols results in almost complete spatial congruence and overlap of activated areas indicating the involvement of similar neuronal populations.

Figure 7 *a* illustrates the mean BOLD MRI response (averaged across subjects) to a single brief (1 s) visual stimulus[22,23]. It not only comprises a rapid signal increase peaking at 6–7 s after the onset of activation, but also shows a signal undershoot relative to pre-stimulation baseline with a minimum about 15–20 s after the onset of activation. Similar to observations for sustained activation, the undershoot phenomenon takes almost 60 s to fully recover and thus indicates that rather long interstimulus periods are required if activation-induced physiologic alterations need to be

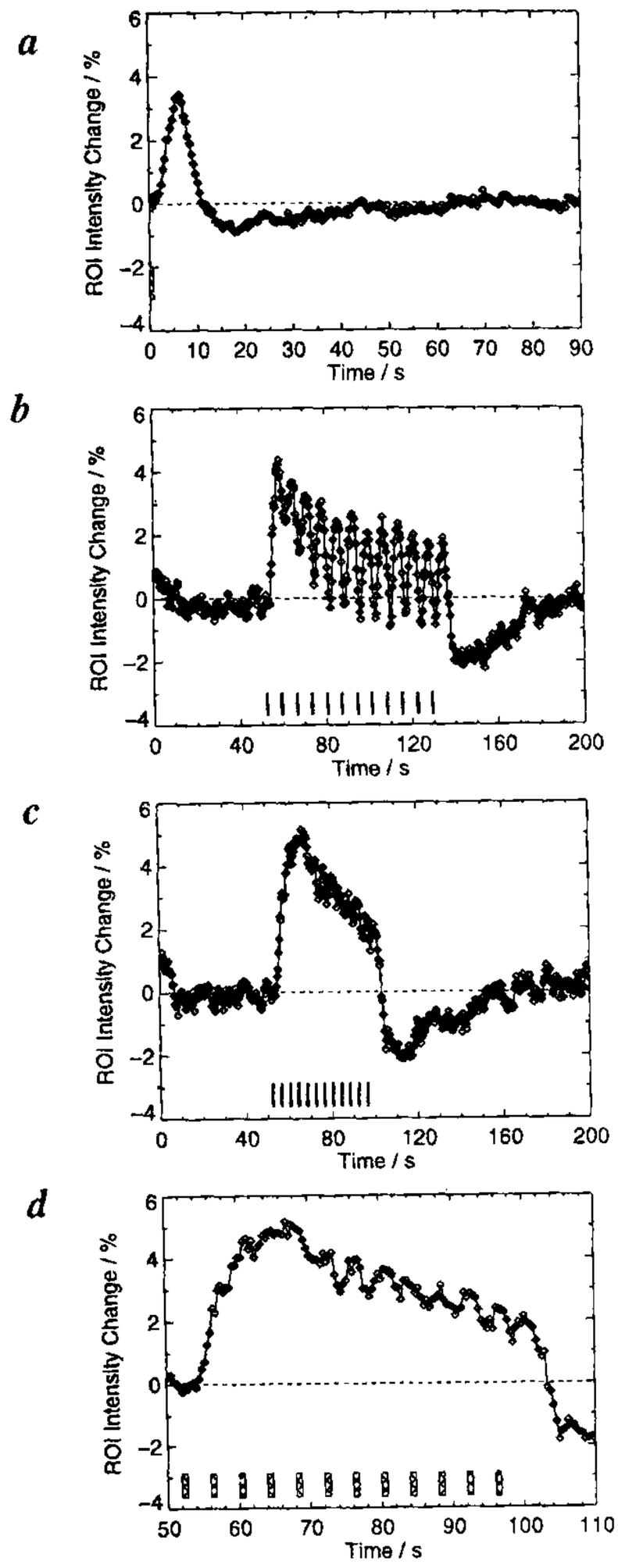

Figure 7*a–d*. Normalized time courses of oxygenation-sensitive MRI signal intensities (2.0 T, EPI, TR/TE = 400/54 ms, flip angle 30°, temporal resolution 0.4 s) for protocols comprising a 1 s period of visual activation (5 Hz reversing black and white checkerboard) and darkness as control. The temporal response characteristics refer to interstimulus periods of ***a***, 89 s; ***b***, 6 s; and ***c***, 3 s; ***d***, Enlarged view of the stimulus-induced responses shown in ***c***. The curves represent mean values of all pixels with statistically significant signal alterations averaged across subjects (n = 6) and stimulation cycles (4–12). (Modified from Fransson, P., *et al.*, *NeuroRep.*, 1998, **9**, 2001–2005.

physiologically 'decoupled' from each other. In fact, even subsecond (200 ms) visual stimuli provide no means for avoiding long-term undershoot responses[24]. However, preliminary experience tells us that physiologic overlap does not alter the resulting activation maps obtained for sustained, single, or repetitive stimulation. On the other hand, the data shown in Figure 7 *a* create an important link between brief cortical events and much slower physiologic fluctuations that modulate the dynamic BOLD MRI signal even in the absence of functional challenge. An analysis of such low frequency 'noise' in the primary sensorimotor and visual system has been used to generate maps of functional connectivity[25].

Event-related mapping

Rather than reducing the stimulus duration we could try to optimize mapping protocols by reducing the duration of interstimulus periods. Pertinent protocols attempt to identify individual 'events' in a stream of rapidly presented stimuli and should facilitate the MRI adaptation of paradigms commonly applied in cognitive neuropsychology. In a baseline study of event-related presentations of identical visual stimuli, we mainly addressed the temporal evolution of the functional contrast and the corresponding ability to generate reliable activation maps[23].

Figures 6 *b* and *c* demonstrate the BOLD MRI responses to repetitive 1 s stimuli when the interstimulus interval is reduced to 6 s or even 3 s, respectively. Figure 6 *d* is a magnification of the central part of Figure 6 *c* as the peak-to-peak signal differences between successive stimulus responses dramatically attenuate for interstimulus durations of less than about 5 s. The real-time response curves indicate that the functional contrast increases from rather low values at the very beginning of repetitive stimulation to a steady-state effect after about 20–30 s. This time is required to benefit from the delayed undershoot contributions of the initial stimuli. The significance of the slow physiologic process is again evidenced by two phenomena: the apparent 'baseline drift' during repetitive stimulation and the pronounced undershoot (–2% signal decrease, 60 s recovery time) afterwards.

Apart from ongoing discussions about a linear or nonlinear system analysis of responses elicited by event-related paradigms, the results confirm our ability to map condition-specific populations of neurons as long as we obtain sufficient functional contrast at the physiologic level (maps not shown). In general, however, complex paradigms may pose further complications because they tend to involve activity switches between arbitrary conditions that may yield both MRI signal increases and decreases. Future work will need to address 'deactivation' at the physiologic level and develop evaluation strategies to analyse bidirectional switches between states of variable degrees of neuronal activity.

Paradigm design

Similar to previous neuroimaging studies using positron emission tomography, most functional MRI examina-

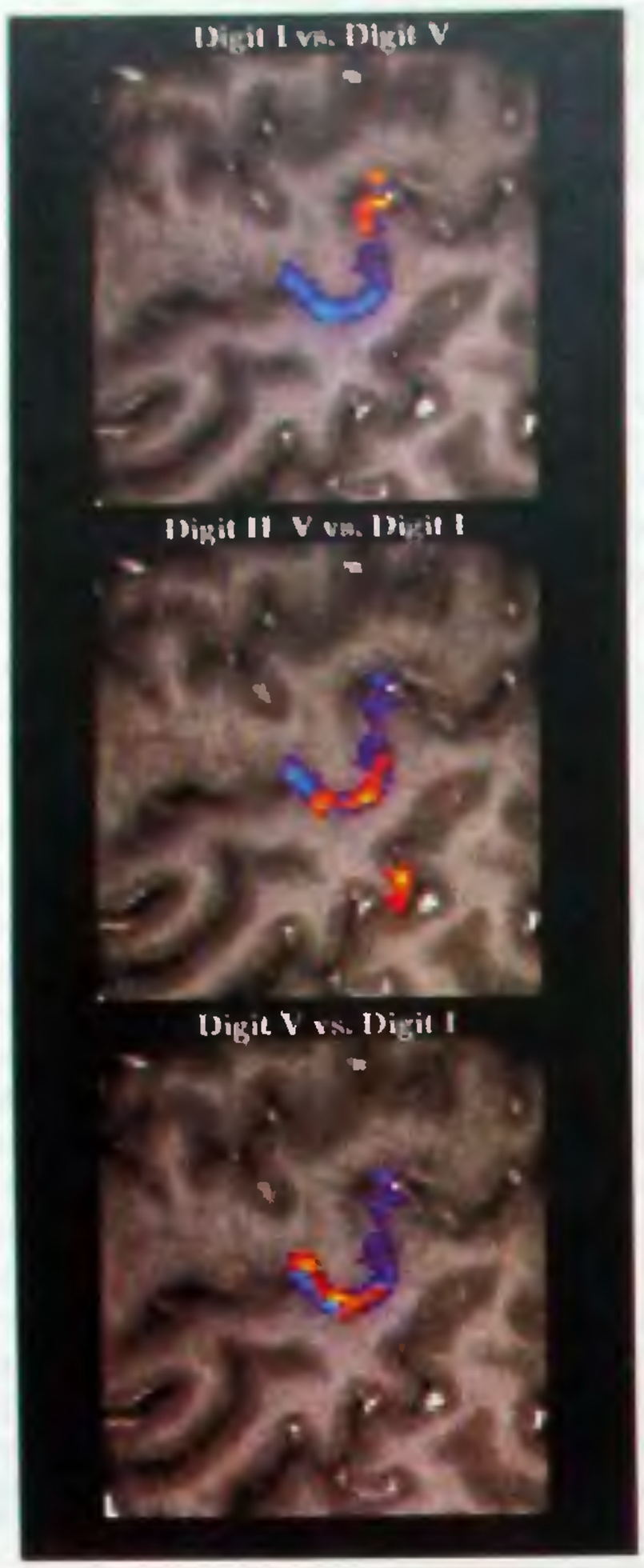

Figure 8. Functional predominance of cortical representations of individual finger movements of the right hand (coded in red) in the left-hemispheric primary motor hand area (coded in blue) of a single right-handed subject. The hand area was delineated by a sequential finger-to-thumb opposition task of the right hand vs motor rest. Despite overlap of representations, functional predominance of the thumb vs little finger (top), index through little finger vs thumb (middle), and little finger vs thumb (bottom) follows a somatotopic arrangement in covering the lateral, intermediate, and medial portion of the hand area, respectively. Functional mapping was accomplished with use of oxygenation-sensitive gradient-echo MRI (2.0 T, FLASH, TR/TE = 62.5/30 ms, flip angle 10°, measuring time 6 s) at high spatial resolution (0.78×1.56 mm^2 interpolated to 0.78×0.78 mm^2 during image reconstruction, section thickness 4 mm). Each dynamic series covered 6 cycles of activation (18 s) and control (36 s). (Modified from Kleinschmidt, A. *et al.*, *Eur. J. Neurosci.*, 1997, **9**, 2178–2186).

tions hitherto employed a simple block structure that compares the neuronal representations of two distinct conditions. This often takes place in the apparently simplified form of combining a truly activated state, (e.g. motor activity, visual stimulation) with a mere control condition (e.g. motor rest, darkness). However, leaving the doubtful assumption of a 'resting' brain, more reasonable concepts adopt the view of qualitatively equivalent states of activity that only quantitatively differ in the degree of neuronal firing or the extent of neuronal populations involved. These ideas lead to the development of interleaved paradigm structures, where multiple conditions may be compared with each other or with suitable combinations thereof.

A simple though illustrative example is the analysis of finger somatotopy in the human motor cortex. Fine-scale somatotopic encoding in brain areas devoted to sensorimotor processing has been questioned by using a perfusion-sensitive MRI technique which suggested its absence within the hand area of the human primary motor cortex[26]. From mostly overlapping representations observed for wrist and various finger movements in a task–rest paradigm, the authors concluded the absence of a somatotopic layout. We re-examined this issue by addressing somatotopy both in terms of functional segregation of cortical representations and of cortical response preference[27].

In a first step, spatial representations of self-paced isolated finger movements were mapped by using motor rest as a control state, i.e. asking for cortical representations in a task–rest design. A subsequent experimental design probed individual finger movements by using contrasting finger movements as control task, i.e. asking for functional predominance of cortical representations in a task1–task2 design. Whereas the first approach confirmed previous reports of extensive overlap in spatial representations (data not shown), the second comparative paradigm revealed foci of differential activation which displayed an orderly medio-lateral progression in accordance with the classical cortical motor homunculus. Examples are depicted in Figure 8 for a single subject at high spatial resolution.

From these design-specific findings it may be concluded that somatotopy within the hand area of the primary motor cortex does not present as qualitative functional segregation but as quantitative predominance of certain digit representations embedded in an overall joint hand area. The data lend support to a refined concept of human motor cortex organization in which large-scale somatotopy exists for separate body parts, whereas fine-scale somatotopy within a physiologically synergetic and anatomically interconnected area is implemented as quantitative predominance of different functions sharing common representations.

Concluding remarks

Magnetic resonance functional neuroimaging bears tremendous scientific and clinical potential. It offers a

noninvasive approach to repeated studies of the functional anatomy of the human brain and thus opens the way to the identification of individualized strategies in higher order processing of single subjects as well as to beneficial applications to patients. In fact, apart from progress in cognitive neuroscience, foreseeable clinical applications range from contributions to presurgical planning to the mapping of disease-related dysfunction and cortical (re-) organization during early brain development or rehabilitation.

Technical limitations originate from the sensitivity to motion and the presence of macroscopic susceptibility artifacts that hamper studies in the vicinity of air–tissue interfaces. Confounding physiologic factors are due to putative modulations of the neurovascular coupling by pharmacologic interventions and brain pathology. Far from being established and a 'safe' tool, ongoing research continues to address all aspects of the mapping process as outlined in Figure 1.

1. Stark, D. D. and Bradley, W. G., *Magnetic Resonance Imaging*, 3rd edition, Mosby, St. Louis, 1998.
2. Bachelard, H. S., in *Advances in Neurochemistry* (eds Agranoff, B. and Suzuki, K.), Plenum, New York, 1997, vol. 8.
3. Ogawa, S., Lee, T. M., Kay, A. R. and Tank, D. W., *Proc. Natl. Acad. Sci. USA*, 1990, **87**, 9868–9872.
4. Turner, R., Le Bihan, D., Moonen, C. T. W., DesPres, D. and Frank, J., *Magn. Reson. Med.*, 1991, **22**, 159–166.
5. Kwong, K. K., Belliveau, J. W., Chesler, D. A., Goldberg, I. E., Weisskoff, R. M., Poncelet, B. P., Kennedy, D. N., Hoppel, B. E., Cohen, M. S., Turner, R., Cheng, H. M., Brady, T. J. and Rosen, B. R., *Proc. Natl. Acad. Sci. USA*, 1992, **89**, 5675–5679.
6. Ogawa, S., Tank, D. W., Menon, R., Ellermann, J. M., Kim, S. G., Merkle, H. and Uğurbil, K., *Proc. Natl. Acad. Sci. USA*, 1992, **89**, 5951–5955.
7. Bandettini, P. A., Wong, E. C., Hinks, R. S., Tikofsky, R. S. and Hyde, J. S., *Magn. Reson. Med.*, 1992, **25**, 390–397.
8. Frahm, J., Bruhn, H., Merboldt, K. D. and Hänicke, W., *J. Magn. Reson. Imaging*, 1992, **2**, 501–505.
9. Blamire, A. M., Ogawa, S., Uğurbil, K., Rothman, D., McCarthy, G., Ellermann, J. M., Hyder, F., Rattner, Z. and Shulman, R. G., *Proc. Natl. Acad. Sci. USA*, 1992, **89**, 11069–11073.
10. Fox, P. T. and Raichle, M. E., *Proc. Natl. Acad. Sci. USA*, 1986, **83**, 1140–1144.
11. Frahm, J., Krüger, G., Merboldt, K. D. and Kleinschmidt, A., *Magn. Reson. Med.*, 1996, **35**, 143–148.
12. Frahm, J., Merboldt, K. D., Hänicke, W., Kleinschmidt, A. and Boecker, H., *NMR Biomed.*, 1994, **7**, 45–53.
13. Frahm, J., Merboldt, K. D. and Hänicke, W., *J. Magn. Reson.*, 1995, **B109**, 234–237.
14. Frahm, J., Merboldt, K. D. and Hänicke, W., *Magn. Reson. Med.*, 1993, **29**, 139–144.
15. Bandettini, P. A., Jesmanowicz, A., Wong, E. C. and Hyde, J. S., *Magn. Reson. Med.*, 1993, **30**, 161–173.
16. Kleinschmidt, A., Requardt, M., Merboldt, K. D. and Frahm, J., *Int. J. Imag. Syst. Technol.*, 1995, **6**, 238–244.
17. Kleinschmidt, A., Bruhn, H., Krüger, G., Merboldt, K. D., Stoppe, G. and Frahm, J., *NMR Biomed.*, 1999, in press.
18. Bruhn, H., Kleinschmidt, A., Boecker, H., Merboldt, K. D., Hänicke, W. and Frahm, J., *J. Cereb. Blood Flow Metab.*, 1994, **14**, 742–748.
19. Kleinschmidt, A., Steinmetz, H., Sitzer, M., Merboldt, K. D. and Frahm, J., *Stroke*, 1995, **26**, 106–110.
20. Krüger, G., Kleinschmidt, A. and Frahm, J., *Magn. Reson. Med.*, 1996, **35**, 797–800.
21. Buxton, R. B., Wong, E. C. and Frank, L. R., *Magn. Reson. Med.*, 1998, **39**, 855–864.
22. Fransson, P., Krüger, G., Merboldt, K. D. and Frahm, J., *Magn. Reson. Med.*, 1998, **39**, 912–919.
23. Fransson, P., Krüger, G., Merboldt, K. D. and Frahm, J., *NeuroRep.*, 1998, **9**, 2001–2005.
24. Fransson, P., Krüger, G., Merboldt, K. D. and Frahm, J., *Magn. Reson. Imag.*, 1999, **17**, 1–7.
25. Biswal, B., Yetkin, F. Z., Haughton, V. M. and Hyde, J. S., *Magn. Reson. Med.*, 1995, **34**, 537–541.
26. Sanes, J. N., Donoghue, J. P., Thangaraj, V., Edelman, R. R. and Warach, S., *Science*, 1995, **268**, 1775–1777.
27. Kleinschmidt, A., Nitschke, M. F. and Frahm, J., *Eur. J. Neurosci.*, 1997, **9**, 2178–2186.

ACKNOWLEDGEMENTS. I thank Harald Bruhn, Peter Fransson, Wolfgang Hänicke, Gunnar Krüger, Andreas Kleinschmidt, and Klaus-Dietmar Merboldt for many invaluable contributions over the past 5 years.